ELSEVIER

Journal of Nuclear Materials 304 (2002) 161–175

journal of nuclear materials

www.elsevier.com/locate/jnucmat

# Thermodynamic assessment of the uranium–oxygen system

C. Guéneau [a,*], M. Baichi [b], D. Labroche [c], C. Chatillon [d], B. Sundman [e]

[a] *DEN/DPC/SCPA CEA-Saclay 91191, Gif-Sur-Yvette cedex, France*
[b] *DEN/DEC/SECI CEA-Grenoble 38054, Grenoble cedex, France*
[c] *DEN/DTE/SIM CEA-Valrho 26702, Pierrelatte cedex, France*
[d] *Laboratoire de Thermodynamique et de Physico-Chimie Métallurgiques (UMR 5614, CNRS-UJF-INPG), 38054 Saint Martin d'Hères, France*
[e] *Department of Materials Science and Engineering, Royal Institute of Technology, S-10044 Stockholm, Sweden*

Received 8 January 2002; accepted 13 May 2002

**Abstract**

A thermodynamic assessment of the uranium–oxygen system is presented. A consistent set of experimental data is selected among the numerous data in the literature on the phase diagram and oxygen chemical potential. The thermodynamic properties of the phases are described using the compound energy model with ionic constituents for the solids and an ionic two-sublattice model for the liquid. For the uranium dioxide, the structure is described using three sublattices, one for the cations $U^{3+}$, $U^{4+}$ and $U^{6+}$, one for the normal site of oxygen ions, and one for the interstitial oxygen ions. Vacancies are included in both oxygen sublattices. In this first approach, the homogeneity ranges of the $U_4O_{9-y}$ and $U_3O_{8-y}$ compounds are not represented. A set of consistent model parameters that describes both the phase diagram and the oxygen chemical potential data in the whole composition range is thus obtained. The description of this basic binary system will be used to calculate higher order systems such as O–U–Zr and Fe–O–U which are important for simulating severe nuclear accidents.


*PACS:* 82.60; 82.60.Cx; 82.60.Fa; 82.60.Hc

## 1. Introduction

The uranium–oxygen system is a key system in the nuclear material field. During a severe nuclear accident, the material resulting from the reactor melting is designated as corium. To predict the heat transfer processes in this complex mixture, the nature and relative fractions of the phases in the solid, liquid or gas state must be known as a function of its composition and temperature. Furthermore, the high temperature evaporation processes have also to be well described. The purpose of the present study is to assess this binary in order to calculate higher order systems such as Fe–O–U, O–U–Zr and Fe–O–U–Zr which are important for the severe nuclear accident studies.

The uranium–oxygen system is characterized by a miscibility gap in the liquid state involving a metallic uranium rich liquid and an oxygen rich liquid, close to the $UO_2$ composition. The dioxide of uranium has a wide composition range at high temperature in which the thermodynamic properties depend on the O/U ratio. The numerous oxidation degrees of uranium lead to the existence of several complex oxides $U_4O_9$, $U_3O_8$ and $UO_3$. THERMODATA (France) and AEA Technology (UK) have developed thermodynamic databases for the corium [1,2] but the model for $UO_{2\pm x}$ in these assessments was not satisfactory. In fact, the $UO_{2+x}$ phase boundary at low temperature ($T < 1400$ K) and the corresponding change of the oxygen chemical potential

* Corresponding author. Tel.: +33-1 69 08 67 41; fax: +33-1 69 08 92 21.
*E-mail address:* cgueneau@cea.fr (C. Guéneau).

0022-3115/02/$ - see front matter 
PII: S0022-3115(02)00878-4

are not well represented. Furthermore, in [1], THERMODATA proposed two sets of thermodynamic parameters for the U–O system corresponding to two different descriptions of the miscibility gap.

The critical analysis of the experimental data by Labroche and Baichi [3,4] allows us to propose a single description of the U–O system. The phases are described using the compound energy model with ionic constituents for the solid phases and an ionic two-sublattice model for the liquid, in order to be consistent with Sundman's assessment of the Fe–O system [5] and the recent work on Zr–O [6]. The present work focusses on the modelling of the thermodynamic properties of $UO_{2\pm x}$. In a later paper, the solubility range of the higher oxides will also be described.

## 2. Selected experimental data

In the present study, the experimental phase diagram and thermodynamic data critically selected by Labroche and Baichi are used for the optimization of the thermodynamic properties of the uranium–oxygen system [3,4]. In the present section, only the selected experimental data are indicated, without any explanation concerning their selection criteria which are detailed in [3,4].

### 2.1. Phase diagram data

The experimental phase diagram data selected for the optimization are listed in Table 1.

In the uranium rich side of the diagram, the experimental data on the oxygen solubility limit in liquid uranium show a strong disagreement [7–12]. The critical analysis of all these experimental investigations has led to select only Edwards and Martin's [7] and Cleaves's [12] data for the optimization. These low oxygen solubility data in liquid uranium are consistent with the experimental tie-line in the liquid miscibility gap determined at $3090 \pm 100$ K [13]. Experimental data on the liquidus and solidus of the $UO_{2-x}$ phase above the mono tectic reaction are available [14–16]. Only Latta and Fryxell's [16] experimental points have been chosen and corrected using the Raoult's cryoscopic law to take into account the decrease of the melting temperature due to the tungsten dissolution in the melt. These data are in good agreement with the average value of $3138 \pm 15$ K selected for the melting point of $UO_2$ [16–19]. The uranium dioxide presents large positive and negative deviations from the stoichiometry. The compound presents an hypostoichiometric domain at temperature above 1500 K. The low oxygen phase boundary data of $UO_{2-x}$ [9,10,20,21] are in good agreement. Other experimental data are rejected for the optimization. For the monotectic reaction [liquid2 = liquid1 + $UO_{2-x}$], the reported temperatures are $2773 \pm 30$ K [7], $2743 \pm 30$ K [9], and $2693 \pm 70$ K [14]. The composition of the liquid2 phase is found at $O/U = 1.3 \pm 0.1$ ($x_O = 0.435$) [7], 1.18 ($x_O = 0.541$) [9] and $1.53 \pm 0.05$ ($x_O = 0.605$) [14]. The O/U ratios of the solid dioxide are in good agreement (1.64 ($x_O = 0.621$) [7], 1.60 ($x_O = 0.615$) [9] and $1.62 \pm 0.06$ ($x_O = 0.618$) [14]).

Table 1
Selection of the U–O phase diagram data

| Data | Authors | References |
|---|---|---|
| Melting point of $UO_2$ | Hein (1968), Kjaerheim (1969) | [53,18] |
| | Latta (1970), Tachibana (1985) | [16,19] |
| Solidus and liquidus of $UO_{2\pm x}$ | Latta (1970) | [16] |
| Liquid miscibility gap tieline | Guéneau (1998) | [13] |
| O solubility in liquid U | Cleaves (1945), Edwards (1966), Blum (1963) | [12,7,8] |
| | Guinet (1966), Pattoret (1969), Garg (1980) | [9–11] |
| $UO_{2-x}$ phase boundary | Martin (1965), Guinet (1966), Pattoret (1969) | [20,9,10] |
| | Ackermann (1965), Ackermann (1969) | [21,72] |
| $UO_{2+x}$ phase boundary | Kiukkola (1962), Markin (1962), Saito (1974) | [29–31] |
| | Marchidan (1972, 1973, 1974, 1975) | [71–74,32] |
| | Gronvold (1955), Schaner (1960) | [33,34] |
| | Aronson (1961), Anthony (1962) | [35,36] |
| | Kotlar (1967a,b, 1968) | [22–24] |
| | Hagemark (1966), Blackburn (1958) | [25,26] |
| | Roberts (1961), Picard (1981) | [27,28] |

In the $UO_2$–O part of the diagram, the $UO_{2+x}$ phase boundary is well known experimentally from 500 to 1950 K [22–36,72–74,86]. The oxygen content in $UO_{2+x}$ increases with temperature up to 1400 K. At this temperature, the $U_4O_9$ phase decomposes to form $U_3O_8$ and $UO_{2+x}$ peritectoidally [26,27,37–40]. The temperature of this peritectoid decomposition of $U_4O_9$ is fixed to $1398 \pm 8$ K [37]. The higher oxygen content of $UO_{2+x}$ is close to the $U_4O_9$ composition, measured up to 1950 K. No information is available between 1950 and 2800 K for the $UO_{2+x}$ composition range and for the invariant reaction [Iiquid2 = $UO_{2+x}$ + Gas]. The $U_4O_9$ oxide presents two second-order transitions at $345 \pm 10$ K [41, 82–84] and $850 \pm 20$ K [42,82,85]. The experimental investigations show that this oxide is slightly hypostoichiometric [22,26–28,34,40]. The temperature of both second-order transitions vary slightly with the O/U ratio. For the $U_3O_8$ oxide, some authors report the existence

of a second phase with the $U_5O_{13}$ formula [43–45]. The composition range of $U_3O_{8-y}$ has been investigated by several authors [23,26,33,44,46–48]. Four crystalline structures of $U_3O_8$ are reported [67]. $UO_3$ does not present any deviation from the stoichiometry. Five crystalline structures are reported for this compound [67].

### 2.2. Thermodynamic data

The selected data for the optimization are listed in Table 2. Numerous experimental data are available for stoichiometric $UO_2$. The selected melting enthalpy of $UO_2$ is equal to $75.4 \pm 2.3$ kJ/mol. This value is consistent with the data reported by Hein, Leibowitz and Rand [49–51]. $UO_2$ heat capacity has been directly determined by Affortit, Mills and Ronchi [79,87,88]. Below 2800 K, Baichi's critical analysis has led to select data from Fink's expression [52]. Above 2800 K, the heat capacity has been deduced from the heat content data of Hein and Leibowitz [53,50]. It gives a constant value of the heat capacity equal to $165.1 \pm 3.3$ J/mol/K of $UO_2$ between 2800 and 3137 K. The peak corresponding to the lambda transition was not taken into account as we consider that this transformation does not occur for stoichiometric $UO_2$ [4]. From 3138 to 3523 K, the heat capacity of liquid $UO_2$ has been taken constant and equal to $131.4 \pm 3.8$ J/mol/K of $UO_2$ according to Hein and Leibowitz [53,54]. Bober and Singer's [55] data giving the boiling temperature of liquid $UO_2$ heated by laser pulses as a function of controlled total pressure in the range 0.025–1 MPa have been used. No other thermodynamic data are reported for the liquid phase. On the contrary, in the solid state, the oxygen potential across the whole composition range of $UO_{2\pm x}$ has been extensively investigated by the emf technique, high temperature mass spectrometry, calorimetry and thermogravimetry. Compatible oxygen chemical potential data for the $UO_{2+x}$ range from 800 to 1800 K have been selected from [22–27,29–32,35,56,57]. In the $UO_{2-x}$ side, three authors have been chosen [10,58,59]. The oxygen chemical potential data in the two-phase liquid U–$UO_{2-x}$ domain, deduced from mass spectrometry measurements performed by Baichi and consistent with Pattoret's data were selected [4,10].

Table 2
Selected experimental U–O thermodynamic data

| Data | Authors | References |
|---|---|---|
| H(T)–H(298 K) of $UO_2$ | Moore (1947), Conway (1965), Ogard (1967) | [75–77] |
| | Hein (1968), Leibowitz (1969), Fredrickson (1970) | [53,50,78] |
| | Leibowitz (1971), Mills (1989), Takahashi (1993) | [54,79,80] |
| O chem. pot. in $UO_{2-x}$ | Tetenbaum (1968), Pattoret (1969), Javed (1972) | [58,10,59] |
| O chem. pot. in $UO_{2+x}$ | Gerdanian (1965), Kotlar (1967a,b, 1968) | [56,22–24] |
| | Hagemark (1966), Roberts (1961), Blackburn (1958) | [25–27] |
| | Aronson (1961), Marchidan (1975), Markin (1962) | [35,32,30] |
| | Saito (1974), Kiukkola (1962), Nakamura (1987) | [31,29,57] |
| O chem. pot. in $UO_{2+x}/U_4O_9$ | Nakamura (1987), Kiukkola (1962), Markin (1962) | [57,29,30] |
| | Blackburn (1958), Kotlar (1967) | [26,22] |
| O chem. pot. in Liquid/ $UO_{2-x}$ | Pattoret (1969), Baichi (2001) | [10,4] |

## 3. Thermodynamic modelling of the phases

In the present study, the oxygen solubilities in the orthorhombic, tetragonal and bcc uranium phases are neglected. The $U_4O_9$, $U_3O_8$ and $UO_3$ oxides are treated as single stoichiometric compounds. A future work will consist in the description of the composition ranges of $U_4O_{9-y}$ and $U_4O_{8-y}$. The Gibbs energy functions for all the phases are referred to the enthalpy of the pure elements, $i$, in their stable state at room temperature 298.15 K and 1 bar ($^0H_i^{SER}(298.15\ K)$).

### 3.1. Pure elements

The Gibbs energy functions of the pure elements $i$ at temperature $T$ and in their state $\varphi$ are given by

$$^0G_i^{\varphi}(T) - {}^0H_i^{SER}(298.15\ K) = a + bT + cT\ln T + \sum d_n T^n, \quad (1)$$

where $n$ is an integer (2, 3, −1, ...). In the present work, Dinsdale's parameters are used for pure uranium [60] and oxygen's data are from SGTE 1997 Substance database [62].

### 3.2. Stoichiometric oxides

The oxides are described with two sublattices, one for the cations and one for the divalent oxygen ions.

#### 3.2.1. $UO_3$

The $UO_3$ oxide is described with the $(U^{6+})_1(O^{2-})_3$ two-sublattice model. The corresponding Gibbs energy function has the same form as in Eq. (1):

$$G^{\varphi}(T) - \sum_i n_i^{\varphi 0} H_i^{SER}(298.15\ K) = a + bT + cT\ln T + \sum d_n T^n, \quad (2)$$

where $n_i^{\varphi}$ is the number of atoms of the $i$th element in the oxide formula. The thermodynamic parameters have been taken from the SGTE 1997 Substance database [62].

*3.2.2. $U_4O_9$ and $U_3O_8$*

For both oxides, a mixture of uranium charged species is assumed in the cation sublattice:

$$(U^{4+}, U^{5+})_4(O^{2-})_9 \quad \text{for } U_4O_9,$$

$$(U^{5+}, U^{6+})_3(O^{2-})_8 \quad \text{for } U_3O_8.$$

The free energy of the oxide with such a sublattice model $(U^{\mu+}, U^{\nu+})_p(O^{2-})_q$ in the state $\varphi$ is expressed by

$$\begin{aligned} G^{\varphi}(T) - p^0H_U^{\mathrm{SER}}(298.15\ \mathrm{K}) - q^0H_O^{\mathrm{SER}}(298.15\ \mathrm{K}) \\ = y_{U^{\mu+}}{}^0G_{U^{\mu+}:O^{2-}} + y_{U^{\nu+}}{}^0G_{U^{\nu+}:O^{2-}} \\ - pRT(y_{U^{\mu+}}\ln y_{U^{\mu+}} + y_{U^{\nu+}}\ln y_{U^{\nu+}}), \end{aligned} \tag{3}$$

where $y_i$, are the site fractions of the cations $i$ in the first sublattice and the ${}^0G_{U^{\mu+}:O^{2-}}$ and ${}^0G_{U^{\nu+}:O^{2-}}$; Gibbs energy functions have the same description as in Eq. (2).

*3.3. Non-stoichiometric dioxide of uranium $UO_{2\pm x}$*

$UO_2$ adopts the fluorite structure which is typical of ionic compounds. The nature of the bonding in $UO_2$ has been controversial for several years. An appreciable degree of covalence is expected in the material. $UO_2$ is known to behave as a semiconductor. The charge-transfer reaction $2U^{4+} = U^{5+} + U^{3+}$ is usually considered [64]. This excitation process is thought to be responsible for the high temperature specific heat excess in the material. But the other charge states $U^{2+}$ and $U^{6+}$ may be also considered. In fact, it seems possible that charge-transfer processes lead to the generation of $U^{2+}$ and $U^{6+}$ as well as $U^{3+}$ and $U^{5+}$ at elevated temperatures. In the present study, the uranium dioxide is described by using the compound energy model with ionic species. The ideal structure of stoichiometric $UO_2$ is described with two sublattices, for $U^{4+}$ and $O^{2-}$ ions respectively.

The hypostoichiometric side of $UO_2$ is modelled by introducing some oxygen vacancies in the normal oxygen sublattice. The charge balance is maintained by the presence of some $U^{3+}$ ions in the uranium sublattice. The experimental studies of the hyperstoichiometric oxide show the presence of two types of interstitial oxygen atoms O′ and O″ in positions that do not correspond to the classical interstitial sites of the fluorite structure [65]. A third sublattice for these interstitial oxygens is added to the two normal sublattices of the fluorite. To maintain the electroneutrality, some $U^{6+}$ cations are introduced in the uranium sublattice. In reality, as reported before, all the charges of uranium +2, +3, +4, +5 and +6 may be introduced in the cation sublattice. But this would considerably complicate the model by increasing the number of parameters to optimize. The structure of the $UO_{2\pm x}$ phase is then described by the following sublattice model:

$$(U^{3+}, U^{4+}, U^{6+})_1(O^{2-}, Va)_2(O^{2-}, Va)_1.$$

The $U^{6+}$ cation was chosen instead of $U^{5+}$ as it allows to have a neutral end point (for the $UO_3$ composition). Moreover, by taking $U^{5+}$, the end composition would be equal to $UO_{2.5}$ that is very close to the real limit of $UO_{2+x}$. This could induce some troubles with the oxygen activities in this composition range of the dioxide. We have done a compromise by choosing $U^{3+}$ to be consistent with the charge transfer reaction.

The number of sites of the interstitial oxygen sublattice is arbitrarily taken to be unity as neighboring sites are excluded due to electrostatic forces and size mismatch. The compound energy model gives the following expression for the Gibbs energy:

$$\begin{aligned} G^{\varphi} - \sum_i n_i^{\varphi 0}H_i^{\mathrm{SER}}(298.15\ \mathrm{K}) \\ = y_3y_Oy'_O{}^0G_{3:O:O} + y_3y_Oy'_V{}^0G_{3:O:V} + y_3y_Vy'_O{}^0G_{3:V:O} \\ + y_3y_Vy'_V{}^0G_{3:V:V} + y_4y_Oy'_O{}^0G_{4:O:O} + y_4y_Oy'_V{}^0G_{4:O:V} \\ + y_4y_Vy'_O{}^0G_{4:V:O} + y_4y_Vy'_V{}^0G_{4:V:V} + y_6y_Oy'_O{}^0G_{6:O:O} \\ + y_6y_Oy'_V{}^0G_{6:O:V} + y_6y_Vy'_O{}^0G_{6:V:O} + y_6y_Vy'_V{}^0G_{6:V:V} \\ + RT(y_3\ln y_3 + y_4\ln y_4 + y_6\ln y_6) + 2RT(y_O\ln y_O \\ + y_V\ln y_V) + RT(y'_O\ln y'_O + y'_V\ln y'_V) + G^E, \end{aligned} \tag{4}$$

where $y_3$, $y_4$ and $y_6$ represent the fractions of uranium with different charges on the metallic sublattice, $y_O$ and $y_V$ are oxygen ions and vacancies respectively on the normal oxygen sublattice, $y'_O$ and $y'_V$ are oxygen ions and vacancies respectively on the interstitial oxygen sublattice. The ${}^0G$ terms correspond to the Gibbs energies of the different compounds formed by considering one

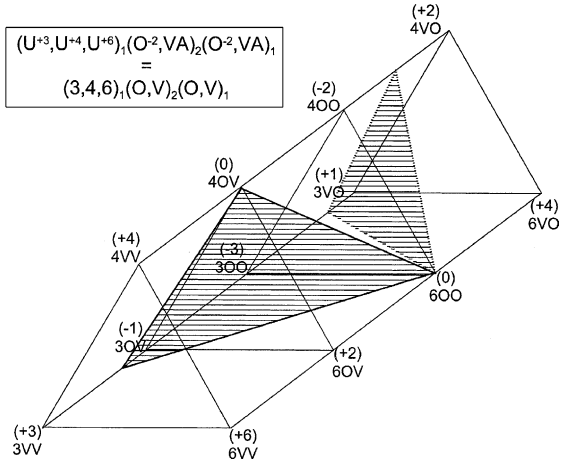


Fig. 1. The sublattice model for solid $UO_{2\pm x}$.

specie in each sublattice. The model is shown as a prism in Fig. 1. The triangular surfaces represent the change of uranium valency with constant occupancy of the other sublattices. Most of the corners correspond to unphysical compounds with a net charge. Among the compounds, the following ones are neutral:

4OV: $(U^{4+})_1(O^{2-})_2(VA)_1$, the ideal fluorite structure of $UO_2$;
6OO: $(U^{6+})_1(O^{2-})_2(O^{2-})_1$, fully filled with the interstitial oxygen ions, of $UO_3$ composition.

By combining oxygen ions and vacancies on the second and third sublattices, other neutral compounds can be generated:

$(U^{4+})_1(O^{2-}_{0.5}, VA_{0.25})_2(O^{2-})_1$ with composition $UO_2$;
$(U^{3+})_1(O^{2-}_{0.75}, VA_{0.25})_2(VA)_1$ with composition $UO_{1.5}$;
$(U^{3+})_1(O^{2-}_{0.25}, VA_{0.75})_2(O^{2-})_1$ with composition $UO_{1.5}$.

By combination of these compounds, the area where the model for the dioxide of uranium is neutral can be determined (the two dashed surfaces with the '6OO' common corner). In each domain, the composition of the phase ranges from $UO_{1.5}$ to $UO_3$. The presence of these two domains shows that with the present model, the dioxide has several internal degrees of freedom, which can give some troubles in the optimization procedure. The surface with the '4OV' corner corresponding to the $UO_2$ ideal fluorite represents the correct domain of stability of the phase. It shows that the most important thermodynamic parameters to optimize are those of the '4OV', '6OO', '3OV' and '3VV' compounds. It was necessary to add an excess Gibbs energy term $G^E$ to describe correctly the phase boundaries of $UO_{2\pm x}$. Some interaction terms $L_i$ were optimized:

$$G^E = (y_3y_4{}^0L_{3,4:O:V} + y_4y_6{}^0L_{4,6:O:V} + y_3y_6{}^0L_{3,6:O:V})y_Oy'_V. \quad (5)$$

The Gibbs energy model for $UO_2$ must be minimized in order to find the fractions of ionic constituents which give the lowest Gibbs energy for each composition.

### 3.4. Liquid phase

The ionic two-sublattice model [66] was adopted for the description of the liquid, with one sublattice for cations and one for anions, hypothetical vacancies with an induced charge and neutral oxygen atoms. The model is

$$(U^{4+})_P(O^{2-}, VA^{-Q}, O)_Q,$$

where $y_{O^{2-}}$, $y_{VA}$ and $y_O$ denote the site fractions of divalent oxygen ions, vacancies and neutral oxygens on the second sublattice. $P$ and $Q$ are equal to the average charge of the opposite sublattice:

$$\begin{aligned} P &= Qy_{VA} + 2y_{O^{2-}}, \\ Q &= 4. \end{aligned} \quad (6)$$

The induced charge of the vacancies corresponds to the average charge of the cation sublattice: $Q = 4$. $P$ varies via the site fractions $y_{O^{2-}}$ and $y_{VA}$ with the composition in order to keep the phase electrically neutral. The Gibbs energy of the liquid phase is given by the following expression:

$$\begin{aligned} G^{liquid} = {} & y_{O^{2-}}{}^0G_{U^{4+}:O^{2-}} + y_{VA}{}^0G_{U^{4+}:VA} + y_O{}^0G_O \\ & + QRT(y_{O^{2-}}\ln y_{O^{2-}} + y_{VA}\ln y_{VA} + y_O\ln y_O) \\ & + y_{O^{2-}}y_{VA}({}^0L_{U^{4+}:O^{2-},VA}) + (y_{O^{2-}} - y_{VA}){}^1L_{U^{4+}:O^{2-},VA} \\ & + (y_{O^{2-}} - y_{VA})^2({}^2L_{U^{4+}:O^{2-},VA}) \\ & + y_{O^{2-}}y_O{}^0L_{U^{4+}:O^{2-},O}, \end{aligned} \quad (7)$$

${}^0G_{U^{4+}:O^{2-}}$, ${}^0G_{U^{4+}:VA}$ and ${}^0G_O$ are the reference terms, corresponding to the Gibbs energy of respectively pure $UO_2$, uranium and fictitious oxygen liquid phases. ${}^0L_{U^{4+}:O^{2-},VA}$, ${}^1L_{U^{4+}:O^{2-},VA}$ and ${}^2L_{U^{4+}:O^{2-},VA}$ are the interaction parameters describing the liquid phase in the U–$UO_2$ composition range. ${}^0L_{U^{4+}:O^{2-},O}$ is added to describe the oxygen enriched liquid.

### 3.5. Gas phase

The gas phase is described as an ideal mixture containing the gaseous species U, O, $O_2$, $O_3$, $O_1U_1$, $O_2U_1$ and $O_3U_1$. The Gibbs energy of the gas phase is given as

$$G^\varphi = \sum_i y_i{}^0G_i^\varphi + RT\sum_i y_i\ln y_i + RT\ln P/P_0, \quad (8)$$

where $y_i$ is the mole fraction of the specie $i$ in the gas phase. ${}^0G_i^\varphi$ represents the standard Gibbs energy of specie $i$ of the gas phase. $R$ is the gas constant, $P_0$ the standard pressure.

## 4. Selection of the adjustable parameters

The least-square optimization program PARROT [63] included in the Thermo Calc databank system [61] was used. The optimization was done in several steps. First, the thermodynamic parameters of the $UO_{2\pm x}$ solid phase were optimized from all the experimental data selected for this phase. Then the equilibria of the dioxide of uranium with $U_4O_9$, $U_3O_8$ and the gas phase were added. When the properties of the dioxide were correctly described, then the parameters of the liquid phase were optimized in order to fit the whole phase diagram data. For all the pure oxide functions, starting values have been taken from SGTE 1997 Substance database [62].

The thermodynamic functions of all phases were allowed to vary in the assessment except those of $UO_3$ that were fixed. The Gibbs energy functions for $U_4O_9$ and $U_3O_8$ compounds have been reoptimized by considering the phase diagram data as well as enthalpy, entropy and thermal capacity data from the SGTE 1997 Substance. The enthalpy and entropy of transition for both oxides are those of the SGTE 1997 Substance, except for the transition at 850 K from $U_4O_9$-S2 to $U_4O_9$-S3 for which an optimization was necessary as this transition is not taken into account in the SGTE database. The adjustable variables are presented in the following section for all the phases.

### 4.1. $UO_{2\pm x}$

The assessment started with describing the $UO_{2\pm x}$ phase field. The experimental heat capacity, enthalpy and entropy data of pure $UO_2$ and oxygen chemical potential data covering the whole composition range of $UO_{2\pm x}$ were used in the optimization procedure. From the model, the stoichiometric $UO_2$ compound is allowed to exhibit some defects such as charge transfer on the uranium sublattice, vacancies on the normal oxygen site and interstitial oxygen ions. With the present model, the heat capacity evolution versus temperature is directly related to the defect fractions. In the composition range of $UO_{2\pm x}$ the oxygen potential $G_{O_2}$ can be calculated as

$$\text{for } UO_{2-x}, \quad \begin{aligned} G_{O_2} &= 4G_{UO_2} - 4G_{UO_{1.5}}, \\ G_{O_2} &= 4G_{4:O:V} - 3G_{3:O:V} - G_{3:V:V}, \end{aligned} \tag{9}$$

$$\text{for } UO_{2+x}, \quad \begin{aligned} G_{O_2} &= 2G_{UO_3} - 2G_{UO_2}, \\ G_{O_2} &= 2G_{6:O:O} - 2G_{4:O:V}. \end{aligned} \tag{10}$$

The chemical potential of one corner (A:B:C) can be calculated by deriving the general equation:

$$G_{A:B:C} = G^{\varphi} + \frac{\partial G^{\varphi}}{\partial y_A} + \frac{\partial G^{\varphi}}{\partial y_B} + \frac{\partial G^{\varphi}}{\partial y_C} - \sum_i y_i \frac{\partial G^{\varphi}}{\partial y_i}. \tag{11}$$

Inserting Eq. (11) in Eq. (9) and neglecting the fractions of $U^{6+}$ and O′ yields for $UO_{2-x}$:

$$\begin{aligned} G_{O_2} &= 4\frac{\partial G^{\varphi}}{\partial y_4} + \frac{\partial G^{\varphi}}{\partial y_O} - \frac{\partial G^{\varphi}}{\partial y_V} - 4\frac{\partial G^{\varphi}}{\partial y_3} - \sum_i y_i \frac{\partial G^{\varphi}}{\partial y_i} \\ &= (4y_O + y_4 - 5y_4y_O)^0G_{4:O:V} \\ &\quad + (4y_V - y_4 - 3y_4y_V)^0G_{4:V:V} \\ &\quad + (y_3 - 4y_O + 3y_3y_O)^0G_{3:O:V} \\ &\quad + (5y_3y_V - y_3 - 4y_V)^0G_{3:V:V} \\ &\quad + RT\ln\frac{y_4^2y_O^2}{y_V^2y_3^4} + 2RT(2y_3\ln y_3 - 2y_4\ln y_4 \\ &\quad + y_V\ln y_V - y_O\ln y_O) + 2RT(2y_3 - 2y_4 + y_V - y_O) \\ &\quad + (4y_3y_O + y_3y_4 - 4y_4y_O - y_3y_4y_O)^0L_{3,4:O:V}. \end{aligned} \tag{12}$$

It shows that the parameters that control the oxygen chemical potential in $UO_{2-x}$ are ${}^0G_{4:O:V}$, ${}^0G_{4:V:V}$, ${}^0G_{3:O:V}$, ${}^0G_{3:V:V}$ and the interaction parameter ${}^0L_{3,4:O:V}$.

For $UO_{2+x}$, neglecting the fractions of $U^{3+}$ and V, the same calculation gives the following expression:

$$\begin{aligned} G_{O_2} &= 2\frac{\partial G^{\varphi}}{\partial y_6} + 2\frac{\partial G^{\varphi}}{\partial y'_O} - 2\frac{\partial G^{\varphi}}{\partial y_4} - 2\frac{\partial G^{\varphi}}{\partial y'_V} - \sum_i y_i \frac{\partial G^{\varphi}}{\partial y_i} \\ &= (2y_6 + 2y'_O - 4y_6y'_O)^0G_{6:O:O} + (4y_4y'_V \\ &\quad - 2y_4 - 2y'_V)^0G_{4:O:V} + (2y'_V - 2y_6)^0G_{6:O:V} \\ &\quad + (2y_4 - 2y'_O)^0G_{4:O:O} + RT\ln\frac{y_6^2y_O'^2}{y_4^2y_V'^2} \\ &\quad + 2RT(y_4\ln y_4 - y_6\ln y_6 + y'_V\ln y'_V - y'_O\ln y'_O) \\ &\quad + 2(y_4y'_V - y_6y'_V - y_4y_6 + y_4y_6y'_V)^0L_{4,6:O:V}. \end{aligned} \tag{13}$$

In the $UO_{2+x}$ side, the oxygen potential is related to the ${}^0G_{6:O:O}$, ${}^0G_{4:O:V}$, ${}^0G_{6:O:V}$, ${}^0G_{4:O:O}$ and ${}^0L_{4,6:O:V}$ parameters.

Each ${}^0G_{A:B:C}$ term is referred to the Gibbs energy of one mole of atoms of $UO_2$:

$${}^0G_{A:B:C} = nG_{U_{1/3}O_{2/3}} + V_i + V_jT, \tag{14}$$

where $n$ is the total number of moles of atoms in one formula unit of ${}^0G_{A:B:C}$ and $V_i$ and $V_j$ are enthalpic and entropic terms to be optimized. The $G_{U_{1/3}O_{2/3}}$ reference term depends on temperature by the following expression:

$$\begin{aligned} G_{U_{1/3}O_{2/3}} &= V70 + V71T + V72T\ln(T) + V73T^2 \\ &\quad + V74T^3 + V75T^{-1}. \end{aligned} \tag{15}$$

As starting values, thermodynamic parameters from SGTE 1997 Substance database were used [62]. In Eq. (4), among the twelve ${}^0G_{A:B:C}$, five ones are independently optimized:

$${}^0G_{4:O:V} = 3G_{U_{1/3}O_{2/3}} + V1 + V2T, \tag{16}$$

$${}^0G_{6:O:O} = 4G_{U_{1/3}O_{2/3}} + V3 + V4T, \tag{17}$$

$${}^0G_{6:O:V} = 3G_{U_{1/3}O_{2/3}} + V5 + V6T, \tag{18}$$

$${}^0G_{3:O:V} = 3G_{U_{1/3}O_{2/3}} + V7 + V8T, \tag{19}$$

$${}^0G_{3:V:V} = G_{U_{1/3}O_{2/3}} + V9. \tag{20}$$

The ${}^0G$ terms with vacancies on the second sublattice and interstitial oxygen anions on the third sublattice are fixed to an arbitrary very high positive value as these terms correspond to unphysical compounds:

$${}^0G_{4:V:O} = {}^0G_{6:V:O} = {}^0G_{3:V:O} = 2G_{U_{1/3}O_{2/3}} + V11. \tag{21}$$

The ${}^0G_{4:O:O}$ and ${}^0G_{3:O:O}$ parameters are related to the other ones by the following expressions:

$${}^0G_{4:O:O} = {}^0G_{4:O:V} + {}^0G_{6:O:O} - {}^0G_{6:O:V} + V13, \quad (22)$$

$${}^0G_{3:O:O} = {}^0G_{3:O:V} + {}^0G_{4:O:O} - {}^0G_{4:O:V}. \quad (23)$$

The ${}^0G_{4:V:V}$ and ${}^0G_{6:V:V}$ terms are connected to ${}^0G_{3:V:V}$ by

$${}^0G_{4:V:V} = {}^0G_{3:V:V} + V17, \quad (24)$$

$${}^0G_{6:V:V} = {}^0G_{3:V:V}. \quad (25)$$

The interaction parameters are independently optimized:

$${}^0L_{3,4:O:V} = V20 + V21T, \quad (26)$$

$${}^0L_{4,6:O:V} = {}^0L_{3,6:O:V} = V23 + V24T, \quad (27)$$

### 4.2. $U_4O_9$ and $U_3O_8$

The ${}^0G$ functions of both stoichiometric oxides (Eq. (3)) are calculated to fit both phase diagram and thermodynamic data of the pure oxides:

For $U_4O_9$:

$$\begin{aligned} {}^0G_{U^{4+}:O^{2-}} &= {}^0G_{U^{5+}:O^{2-}} \\ &= V79 + V80T + V81T\ln(T) \\ &\quad + V82T^2 + V83T^{-1}, \end{aligned} \quad (28)$$

For $U_3O_8$:

$$\begin{aligned} {}^0G_{U^{5+}:O^{2-}} &= {}^0G_{U^{6+}:O^{2-}} \\ &= V84 + V85T + V86T\ln(T) \\ &\quad + V87T^2 + V88T^{-1}. \end{aligned} \quad (29)$$

### 4.3. Liquid phase

In Eq. (7), the Gibbs energy functions of pure uranium and oxygen liquid phases are taken from the Substance SGTE 1997 database [61,62]. The Gibbs energy function of stoichiometric $UO_2$ liquid is expressed as

$$\begin{aligned} {}^0G_{U^{4+}:O^{2-}} &= V90 + V91T + V92T\ln(T) \\ &\quad + V93T^2 + V94T^{-1}. \end{aligned} \quad (30)$$

As starting values, parameters from the Substance SGTE 1997 database [61,62] were used. The following interaction parameters are optimized:

in the U–$UO_2$ part

$${}^0L_{U^{4+}:O^{2-},VA} = V30 + V31T, \quad (31)$$

$${}^1L_{U^{4+}:O^{2-},VA} = V32 + V33T, \quad (32)$$

$${}^2L_{U^{4+}:O^{2-},VA} = V34 \quad (33)$$

in the $UO_2$–O part

$${}^0L_{U^{4+}:O^{2-},O} = V40. \quad (34)$$

### 4.4. Gas phase

The Gibbs energy of all the gas species are taken from the Substance SGTE 1997 database [61,62]. Some variables have been added for some gas species in order to allow a slight variation of these parameters to improve the fit of the experimental data:

$${}^0G_{U_1O_3} = {}^0G_{U_1O_3,SGTE1997} + V62, \quad (35)$$

$${}^0G_{U_1O_2} = {}^0G_{U_1O_2,SGTE1997} + V61, \quad (36)$$

$${}^0G_{U_1O_1} = {}^0G_{U_1O_1,SGTE1997} + V60. \quad (37)$$

## 5. Results and discussion

The resulting set of parameters for the U–O system is shown in Table 3. The related calculated uranium–oxygen phase diagram at 1 bar is given in Fig. 2. The calculated standard enthalpy, entropy and heat capacity of the stoichiometric oxides at 298.15 K are presented in Table 4. The properties of the stoichiometric oxides are in good agreement with the experimental data selected in [67] that are consistent with the Substance SGTE 1997 database and with the experimental data selected in the present work.

### 5.1. Stoichiometric $UO_2$ properties

The calculated heat content H(T)–H(298 K) of stoichiometric $UO_2$ versus temperature is in good agreement with the experimental data selected in the present study as shown in Fig. 3. The calculated melting enthalpy value of 78.7 kJ/mol of $UO_2$ is slightly higher than the experimental one: $75.4 \pm 2.3$ kJ/mol. Fig. 4 presents the calculated heat capacity versus temperature in comparison with the selected experimental data. The increasing of the heat capacity around 2000 K is well represented and can be directly connected to the corresponding

Table 3
Calculated thermodynamic parameters of the U–O system (values in J, K, mol)

| | |
|---|---|
| Liquid | $(U^{4+})_P(O^{2-},VA^{-Q},O)_4$ |
| Pure $UO_2$ | ${}^0G_{U^{4+}:O^{2-}} - 4\,{}^0H_O^{SER} - 2{}^0H_U^{SER} = 2GUO_2LIQ$ |
| Fictitious pure O | ${}^0G_{U^{4+}:O} - {}^0H_O^{SER} = {}^0G_O^{SER} - 2648.93 + 31.44T$ |
| Pure U | ${}^0G_{U^{4+}:VA} - {}^0H_U^{SER} = {}^0G_U^{SER} + 12355.5 - 10.3239T$ |
| | ${}^0L_{U^{4+}:O^{2-},VA} = 1655637 - 483.896T$ |
| | ${}^1L_{U^{4+}:O^{2-},VA} = 169888.5 - 148.417T$ |
| | ${}^2L_{U^{4+}:O^{2-},VA} = -394257$ |
| | ${}^0L_{U^{4+}:O^{2-},O} = -350000$ |
| with $GUO_2LIQ$ | $= -1277931.2 + 1255.6513T - 176.41104T\ln T + 6.24183\ 10^{-3}T^2 + 1.0533049\ 10^8T^{-1}$ |
| FCC $UO_{2\pm x}$ | $(U^{3+},U^{4+},U^{6+})_1(O^{2-},VA)_2(O^{2-},VA)_1$ |
| | ${}^0G_{4:O:V} - {}^0H_U^{SER} - 2{}^0H_O^{SER} = 3G_{U_{1/3}O_{2/3}} - 1680662 - 244.203T$ |
| | ${}^0G_{6:O:O} - {}^0H_U^{SER} - 3{}^0H_O^{SER} = 4G_{U_{1/3}O_{2/3}} - 1873393 - 295.669T$ |
| | ${}^0G_{6:O:V} - {}^0H_U^{SER} - 2{}^0H_O^{SER} = 3G_{U_{1/3}O_{2/3}} - 1194847 - 209.893T$ |
| | ${}^0G_{3:O:V} - {}^0H_U^{SER} - 2{}^0H_O^{SER} = 3G_{U_{1/3}O_{2/3}} - 1713747 - 301.572T$ |
| | ${}^0G_{3:V:V} - {}^0H_U^{SER} = G_{U_{1/3}O_{2/3}} + 99409.77$ |
| | ${}^0G_{6:V:O} - {}^0H_U^{SER} - {}^0H_O^{SER} = 2G_{U_{1/3}O_{2/3}} + 1000000$ |
| | ${}^0G_{4:V:O} - {}^0H_U^{SER} - {}^0H_O^{SER} = 2G_{U_{1/3}O_{2/3}} + 1000000$ |
| | ${}^0G_{3:V:O} - {}^0H_U^{SER} - {}^0H_O^{SER} = 2G_{U_{1/3}O_{2/3}} + 1000000$ |
| | ${}^0G_{4:O:O} - {}^0H_U^{SER} - 3{}^0H_O^{SER} = 4G_{U_{1/3}O_{2/3}} - 2788112 - 329.979T$ |
| | ${}^0G_{3:O:O} - {}^0H_U^{SER} - 3{}^0H_O^{SER} = 4G_{U_{1/3}O_{2/3}} - 2821197 - 387.348T$ |
| | ${}^0G_{4:V:V} - {}^0H_U^{SER} = G_{U_{1/3}O_{2/3}} + 556545.7$ |
| | ${}^0G_{6:V:V} - {}^0H_U^{SER} = {}^0G_{3:V:V}$ |
| | ${}^0L_{3,4:O:V} = -67521 + 13.059T$ |
| | ${}^0L_{4,6:O:V} = {}^0L_{3,6:O:V} = 291812.2 - 30.3811T$ |
| with $G_{U_{1/3}O_{2/3}}$ | $= 187258.2 + 266.51073T - 31.08206T\ln T + 3.3558\ 10^{-3}T^2 - 6.80382\ 10^{-7}T^3 + 382076.4T^{-1}$ |
| $U_4O_9$ | $(U^{4+},U^{5+})_4(O^{2-})_9$ with $y_{U^{4+}} = y_{U^{5+}} = 0.5$ |
| | ${}^0G_{U^{4+}:O^{2-}} - 4{}^0H_U^{SER} - 9{}^0H_O^{SER} = G_{U_4O_9}$ |
| | ${}^0G_{U^{5+}:O^{2-}} - 4{}^0H_U^{SER} - 9{}^0H_O^{SER} = G_{U_4O_9}$ |
| | $G_{U_4O_9} = -4616473 + 1811.0382T - 311.209T\ln(T) - 0.03113T^2 + 1741269T^{-1}$ |
| | $G_{U_4O_9-S} = G_{U_4O_9}$ |
| | $G_{U_4O_9-S_2} = G_{U_4O_9} + 2594 - 7.45402T$ |
| | $G_{U_4O_9-S_3} = G_{U_4O_9} + 2684.25 - 7.5602T$ |
| $U_3O_8$ | $(U^{5+},U^{6+})_3(O^{2-})_8$ with $y_{U^{5+}} = 2/3$ and $y_{U^{6+}} = 1/3$ |
| | ${}^0G_{U^{5+}:O^{2-}} - 3{}^0H_U^{SER} - 8{}^0H_O^{SER} = G_{U_3O_8}$ |
| | ${}^0G_{U^{6+}:O^{2-}} - 3{}^0H_U^{SER} - 8{}^0H_O^{SER} = G_{U_3O_8}$ |
| | $G_{U_3O_8} = -3674804 + 1616.3775T - 276.748T\ln(T) - 0.013664T^2 + 2036667T^{-1}$ |
| | $G_{U_3O_8-S} = G_{U_3O_8}$ |
| | $G_{U_3O_8-S2} = G_{U_3O_8} + 135 - 0.279503T$ |
| | $G_{U_3O_8-S3} = G_{U_3O_8} + 283 - 0.5400665T$ |
| | $G_{U_3O_8-S4} = G_{U_3O_8} + 597 - 0.9183797T$ |
| $U_1O_3$ | $(U^{6+})_1(O^{2-})_3$ |
| | ${}^0G_{UO_3-S} - {}^0H_U^{SER} - 3{}^0H_O^{SER} = G_{UO_3}^{SGTE\ 97}$ |
| | $G_{UO_3}^{SGTE\ 1997} = -1260394.6 + 616.4757T - 105.737T\ln(T) + 0.010427T^2$ $-3.18099\ 10^{-6}\ T^3 + 868736\ T^{-1}$ |
| Gas | (U, O, $O_2$, $O_3$, $U_1O_1$, $U_1O_2$, $U_1O_3$) |
| | ${}^0G_{U(g)} - {}^0H_U^{SER} = G_{U(g)}^{SGTE\ 97}$ |
| | ${}^0G_{O(g)} - {}^0H_O^{SER} = G_{O(g)}^{SGTE\ 97}$ |
| | ${}^0G_{O_2(g)} - 2{}^0H_O^{SER} = G_{O_2(g)}^{SGTE\ 97}$ |
| | ${}^0G_{O_3(g)} - 3{}^0H_O^{SER} = G_{O_3(g)}^{SGTE\ 97}$ |
| | ${}^0G_{U_1O_1(g)} - {}^0H_O^{SER} - {}^0H_U^{SER} = G_{U_1O_1(g)}^{SGTE\ 97} - 15000$ |
| | ${}^0G_{U_1O_2(g)} - 2{}^0H_O^{SER} - {}^0H_U^{SER} = G_{U_1O_2(g)}^{SGTE\ 97} + 3300$ |
| | ${}^0G_{U_1O_3(g)} - 3{}^0H_O^{SER} - {}^0H_U^{SER} = G_{U_1O_3(g)}^{SGTE\ 97} + 4800$ |
| | For U species, SGTE 97: Thermo Center of the Russian Academy of Science |

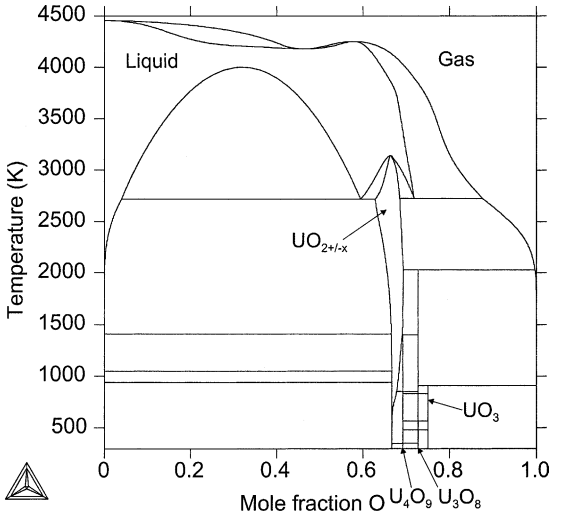


Fig. 2. Calculated phase diagram for U–O at 1 bar.

Table 4
Calculated standard enthalpy, entropy and heat capacity of the stoichiometric oxides at 298.15 K in J/mol of atom-comparison with selected data in [67] that are consistent with the SGTE Substance database 1997 [61]

| Oxide | | $\Delta H_f$ (298 K) | $S^0$ (298 K) | $C_p^0$ (298 K) |
|---|---|---|---|---|
| $UO_2$ (s) | Calc. | −361 374 | 25.65 | 20.98 |
| | Select. | −361 667 ± 333 | 25.68 ± 0.07 | 21.2 ± 0.03 |
| $U_4O_9$ (s) | Calc. | −346 864 | 25.73 | 22.35 |
| | Select. | −347 077 ± 523 | 25.70 ± 0.5 | 22.57 ± 0.05 |
| $U_3O_8$ (s) | Calc. | −325 220 | 25.83 | 21.73 |
| | Select. | −324 979 ± 218 | 25.68 ± 0.05 | 21.63 ± 0.04 |
| $UO_3$ (s) | Calc. | −305 950 | 24.03 | 20.42 |
| | Select. | −304 375 ± 750 | 24.92 ± 0.33 | 20.46 ± 0.07 |
| U (g) | Calc. | +534 996 | 199.8 | 23.69 |
| | Select. | +533 000 ± 8000 | 199.8 ± 0.1 | 23.69 ± 0.04 |
| UO (g) | Calc. | +7954 | 126.1 | 19.67 |
| | Select. | +15 250 ± 8500 | 124.4 ± 1.0 | 21.0 ± 1.0 |
| $UO_2$ (g) | Calc. | −158 176 | 88.8 | 19.84 |
| | Select. | −159 267 ± 6667 | 88.8 ± 1.33 | 19.83 ± 0.67 |
| $UO_3$ (g) | Calc. | −198 613 | 77.4 | 16.12 |
| | Select. | −199 800 ± 375 | 77.4 ± 0.5 | 16.12 ± 0.5 |

variation of the calculated $U^{6+}$ and $U^{3+}$ fractions as shown in Fig. 5. With our sublattice model, it was im-

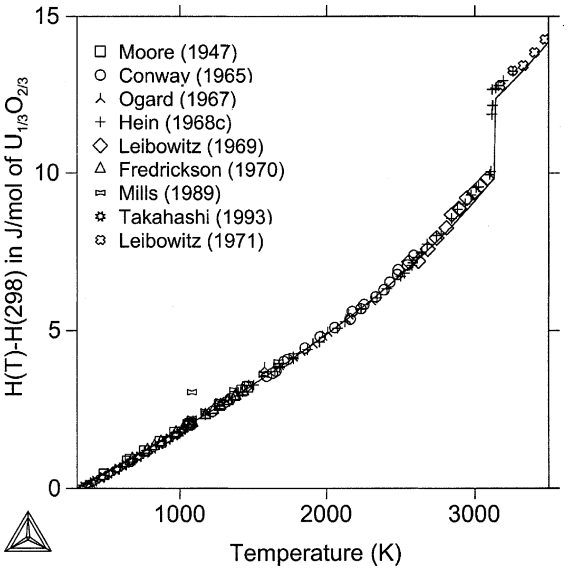


Fig. 3. Calculated heat content together with experimental data.

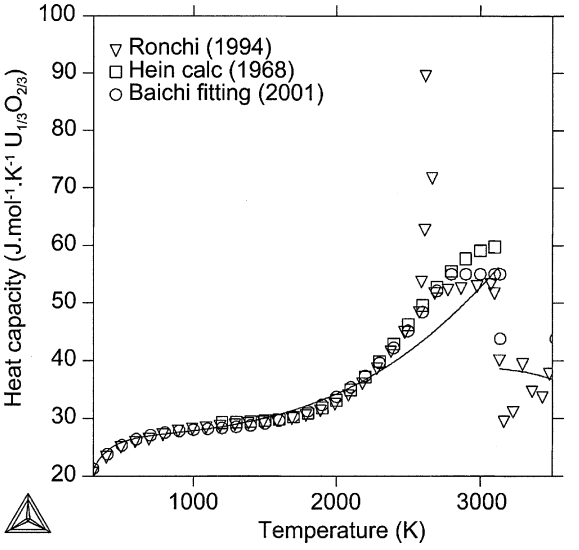


Fig. 4. Calculated heat capacity together with Ronchi's data; estimated values from Hein's heat content experimental data as well as Baichi's fitting.

possible to have a constant value of the heat capacity from 2800 K to the melting point, as it was recommended in the critical review of the experimental data. In fact, with our model, it is not possible to represent a break point in the heat capacity curve without entering a phase transformation. Furthermore, a constant heat capacity may correspond to a constant defect fraction

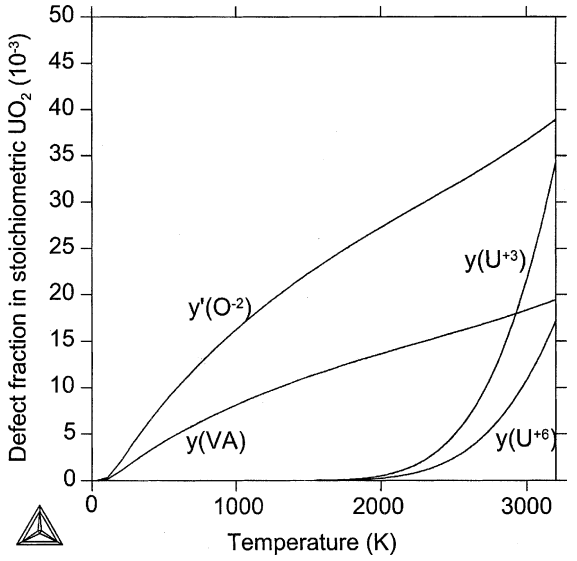


Fig. 5. Calculated defect fraction in stoichiometric $UO_2$ versus temperature.

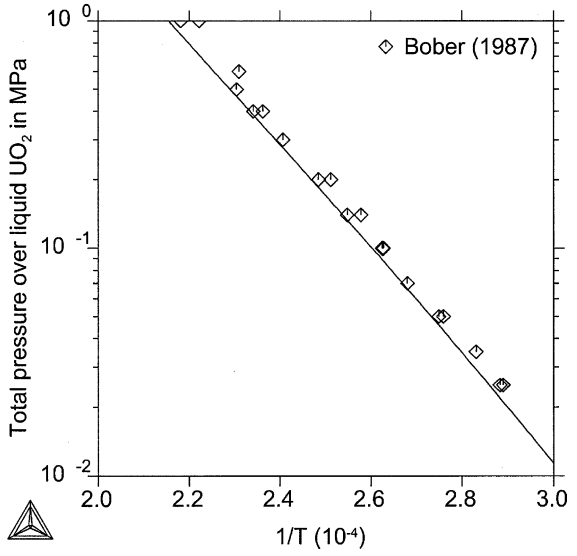


Fig. 6. Calculated total pressure over liquid $UO_2$ versus reciprocal temperature in comparison with Bober and Singer's data [55].

which is inconsistent with our model. Consequently, the agreement between calculation and experiments is less good from 2500 K to the melting point. The calculated total pressure of the gas over liquid $UO_2$ versus reciprocal temperature is compared with Bober's data in Fig. 6. The agreement is very good.

### 5.2. Oxygen chemical potential in $UO_{2\pm x}$

In Fig. 7, the calculated oxygen partial pressures in the single-phase $UO_{2\pm x}$ are compared to the experimental data deduced from the critical review between 800 and 2700 K. The agreement is very good in the whole composition and temperature range. The three sublattice model used to describe the uranium dioxide reproduces well the variation of the oxygen chemical potential. Fig. 8 presents the corresponding variation of the constituent fractions in the different sublattices of the model versus oxygen concentration at 2400 K. The major defects in $UO_{2-x}$ are the oxygen vacancies in connection with a charge transfer in the cation sublattice, leading to the presence of $U^{3+}$ cations. The fraction of $U^{3+}$ decreases with oxygen concentration. In the $UO_{2+x}$ composition range, the major defects are interstitial oxygen anions in connection with the presence of $U^{6+}$ in the cation sublattice. The calculated chemical potential data in the two phase $UO_{2+x}$–$U_4O_9$, $U_4O_9$–$U_3O_8$ and $UO_{2+x}$–$U_3O_8$ as well as liquid U–$UO_{2-x}$ domains are in good agreement with the selected experimental data as shown respectively in Figs. 9 and 10. The calculated oxygen partial pressures in all two-phase regions of the phase diagram are presented in Fig. 11.

### 5.3. Phase diagram

Fig. 12 shows the calculated phase diagram in comparison with the experimental points in the U–$UO_2$ part. An overall good agreement is obtained. The calculated compositions and temperatures of all invariant reactions are presented in Table 5. The calculated congruent melting point of $UO_2$ is equal to 3142 K for a O/U ratio of 1.98. These results are consistent with the selected experimental data of $3138 \pm 23$ K for the temperature. The calculated O/U ratio is a little bit too low but is still within the experimental uncertainty on the oxide composition at melting, $\pm 0.02$ [4]. The calculated boiling temperature of liquid $UO_2$ is equal to 3842 K which is consistent with the experimental values of 3820 K from Benezech [68] and of 3817 K from Breitung [69]. In our study, the boiling point of liquid $UO_2$ is not congruent. In fact, there are two azeotropic compositions, one maximum and one minimum (when regarding temperature) at constant pressure. This behaviour corresponds to the congruent vaporization as observed for $UO_{2-x}$ in experiments under vacuum (or effusion) conditions [10,21,81]. This tendency goes on at high temperature for the equilibrium between liquid and gas [4]. In our assessment, the congruency liquid/gas appears for an oxygen mole fraction of 0.58 for 1 bar total pressure as shown in Fig. 2. Furthermore, in the experimental investigations of the boiling point of liquid $UO_2$, the congruency is supposed but the final liquid composition is never measured. At low temperature, the limit of the hyperstoichiometric

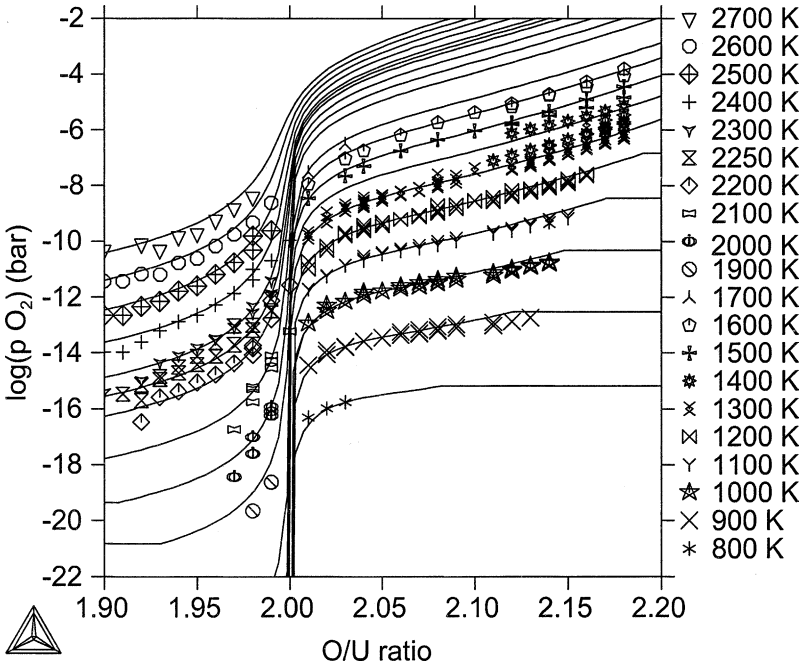


Fig. 7. Calculated oxygen activities in $UO_{2\pm x}$ with selected experimental data (see Table 2).

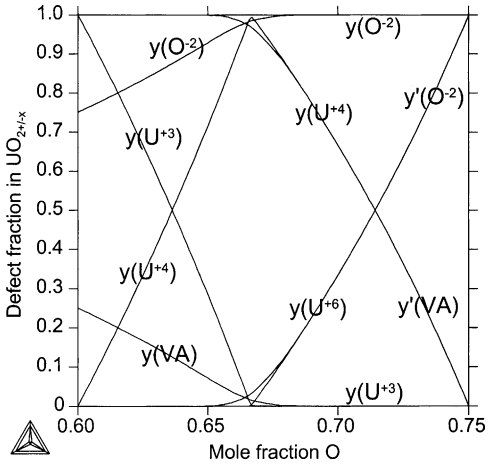


Fig. 8. Calculated fraction of defects as a function of comparison at 2400 K in $UO_{2\pm x}$.

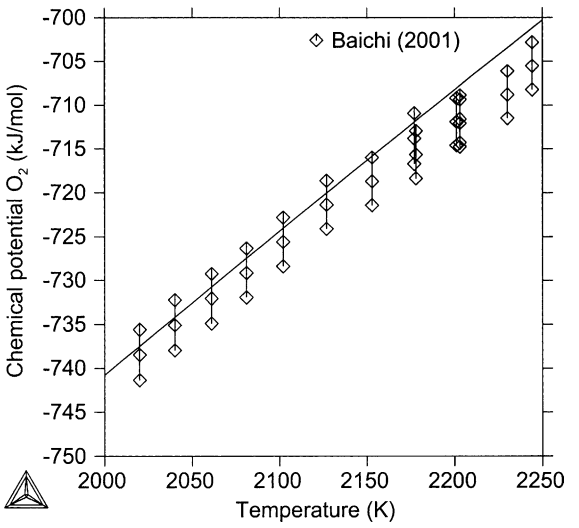


Fig. 9. Calculated chemical potential in the two-phase (liquid U (sat. O)–$UO_{2\pm x}$) domain versus temperature.

composition domain of the dioxide is well reproduced as shown in Fig. 13, displaying the domain of stability of the uranium dioxide. In the ($U_4O_9$–$UO_{2+x}$) two-phase field, the oxygen solubility limit remains relatively flat until 800–900 K. This can be related to a tendency to the demixing of $UO_2$, which is consistent with the oxygen activity curves in Fig. 7. Moreover, experimental investigations show that the $U_4O_9$ structure can be described as an arrangement of cuboctahedric oxygen defects in a fluorite crystal with a parameter equal to four times the one of $UO_2$ and a composition of $UO_{2.23}$ (compared to $UO_{2.25}$) [70]. In this way, $U_4O_9$ could be modelled as the same phase as $UO_2$ that would demix for a limiting oxygen content. This could explain both phase diagram and thermodynamics at low temperature in this composition range. It shows that the $U_4O_9$ phase is complex and requires other investigations to better understand this domain of the phase diagram.

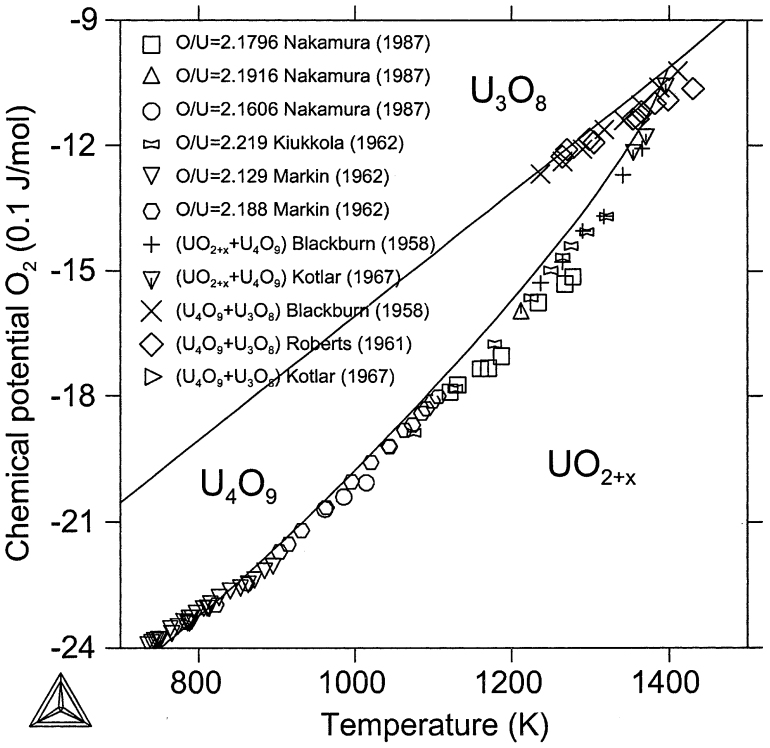


Fig. 10. Calculated chemical potential in the two-phase ($UO_{2\pm x}$–$U_4O_9$) and ($U_4O_9$–$U_3O_8$) domains versus temperature.

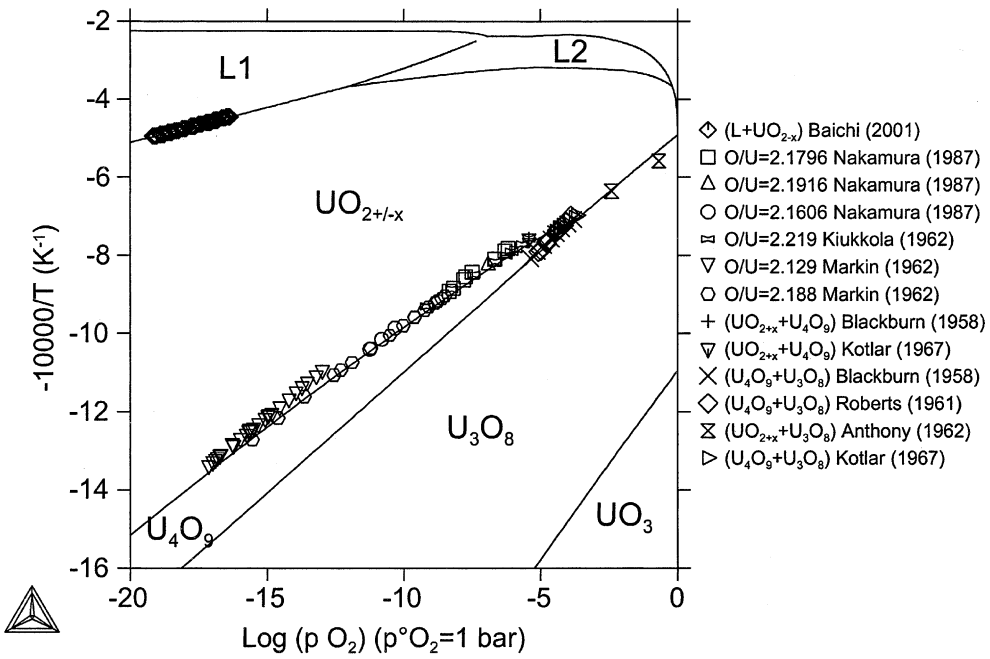


Fig. 11. Calculated oxygen partial pressure in the phase diagram versus reciprocal temperature.

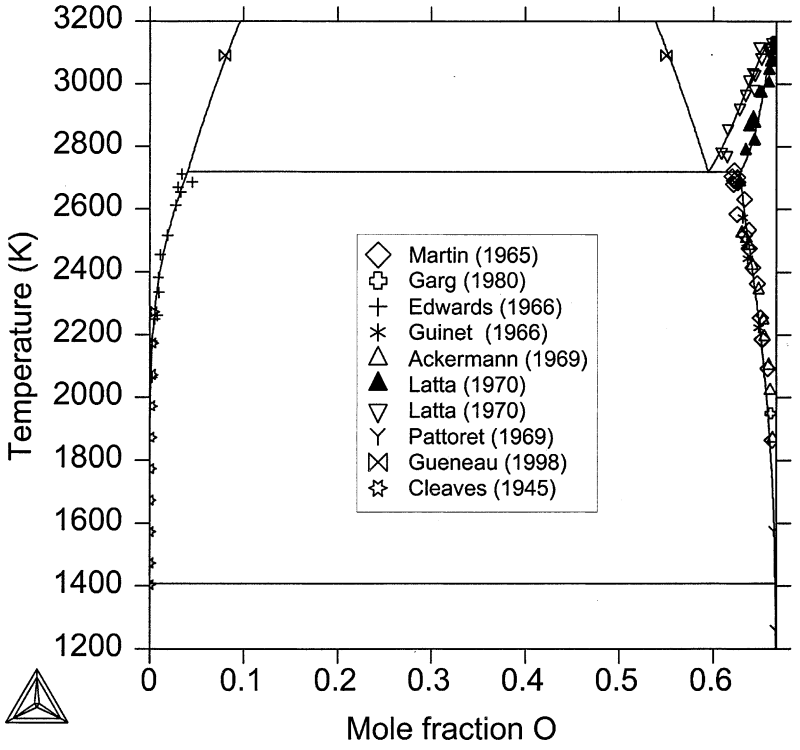


Fig. 12. Calculated phase diagram in U–$UO_2$ side with experimental data.

Table 5
Calculated temperatures and oxygen compositions for all invariant reactions

| T (K) | Invariant transformation (mole fraction O) |
|---|---|
| 4252 | Liquid (0.58) = Gas (0.58) |
| 4182 | Liquid (0.46) = Gas (0.46) |
| 3142 | $UO_2$ (0.664) = Liquid (0.664) |
| 2727 | Liquid (0.719) = $UO_{2+x}$ (0.685) + Gas (0.875) |
| 2719 | Liquid 2 (0.594) = Liquid 1 (0.040) + $UO_{2-x}$ (0.628) |
| 2032 | $U_3O_8$-S4 (0.727) = $UO_{2+x}$ (0.693) + Gas (0.996) |
| 1408 | Liquid ($2 \times 10^{-7}$) = U-bcc (0) + $UO_{2-x}$ (0.665) |
| 1399 | $U_4O_9$-S3 (0.692) = $UO_{2+x}$ (0.691) + $U_3O_8$-S4 (0.727) |
| 1049 | U-bcc (0) = U-tetragonal (0) + $UO_{2-x}$ (0.666) |
| 942 | U-tetragonal (0) = U-orthorhombic (0) + $UO_{2-x}$ (0.667) |
| 913 | $UO_3$ (0.75) = $U_3O_8$-S4 (0.727) + Gas (1.0) |
| 850 | $U_4O_9$-S3 (0.692) = $U_4O_9$-S2 (0.692) |
| 830 | $U_3O_8$-S4 (0.727) = $U_3O8$-S3 (0.727) |
| 598 | $UO_3$ (0.75) = $U_3O_8$-S (0.727) + Gas (1.0) |
| 568 | $U_3O_8$-S3 (0.727) = $U_3O_8$-S2 (0.727) |
| 483 | $U_3O_8$-S2 (0.727) = $U_3O_8$-S (0.727) |
| 348 | $U_4O_9$-S2 (0.692) = $U_4O_9$-S (0.692) |
| 1878 | $U_3O_8$-S4 decomposition in air |
| 861 | $UO_3$ decomposition in air |

## 6. Conclusion

The uranium–oxygen system was assessed on the basis of the critical review of the experimental data performed by Labroche and Baichi in their thesis work. A consistent set of experimental data was selected among the numerous data on the phase diagram and oxygen chemical potential. In the present work, these experimental data are used to optimize the thermodynamic properties of the uranium–oxygen system. The properties of the phases were described using the compound energy model with ionic constituents for the solids and an ionic two-sublattice model for the liquid. For the uranium dioxide, the structure is described using three sublattices, one for the cations $U^{3+}$, $U^{4+}$ and $U^{6+}$, one for the normal site of oxygen, and one for the interstitial divalent oxygen ions. Vacancies are included in both sublattices. A set of consistent model parameters was obtained that describes successfully both the phase diagram and the oxygen chemical potential data in the whole composition range. It shows that the three sublattice model is suitable to describe complex oxides such as $UO_{2\pm x}$. To continue this work, the homogeneity ranges of the $U_4O_{9-y}$ and $U_3O_{8-y}$ compounds will be represented in a future assessment. Concerning the experimental data critical review, there still remain some

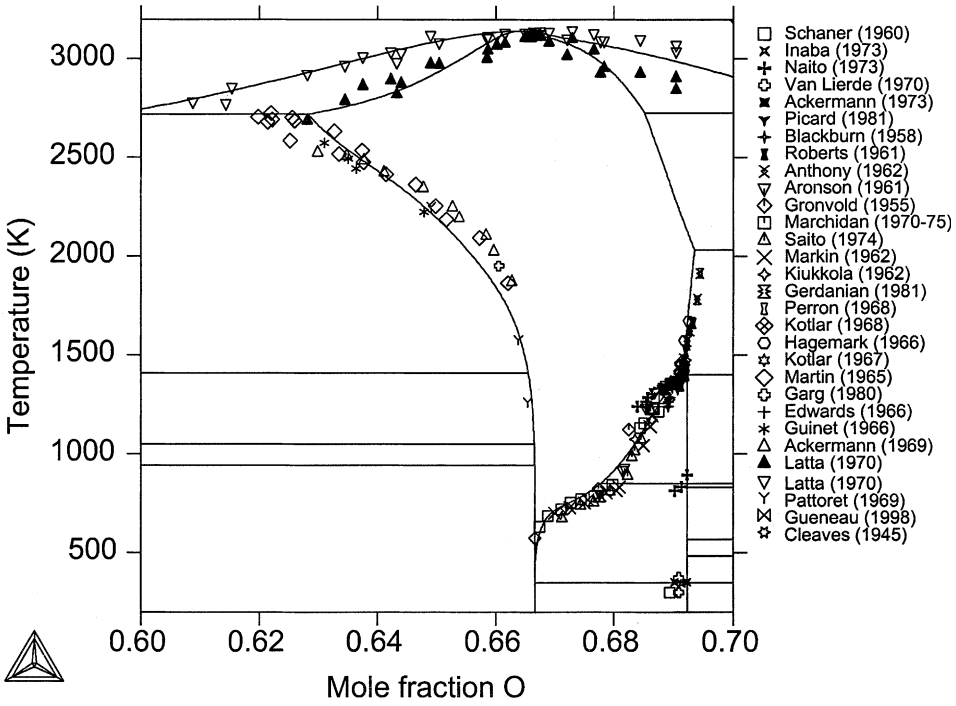


Fig. 13. Calculated phase diagram in $UO_{2\pm x}$ domain with experimental data.

inconsistencies on the thermodynamic data of the gas species UO, $UO_2$ and $UO_3$ (enthalpy, entropy and heat capacity and partial pressure). In the next assessment, these gas properties are to be fixed on the basis of a critical review in order to improve the description of the congruent equilibria between the condensed and gas phases. The present description of this basic binary system will be used to calculate higher order systems such as O–U–Zr and Fe–O–U which are important for simulating severe nuclear accidents.

## Acknowledgements

The authors want to thank M. Rand for having spent much time with our paper and for his advices based on his long experience on uranium chemical thermodynamics.

## References

[1] P.Y. Chevalier, E. Fischer, J. Nucl. Mater. 257 (1998) 213.
[2] M. Rand, personal communication.
[3] D. Labroche, PhD thesis, INPG Grenoble, 2000.
[4] M. Baichi, PhD thesis, INPG Grenoble, 2001.
[5] B. Sundman, J. Phasse Equ. 12 (1991) 127.
[6] P. Liang, N. Dupin, S.G. Fries, H.J. Seifert, I. Ansara, H.L. Lukas, F. Aldinger, Z. Metallkd. 92 (2001) 747.
[7] R.K. Edwards, A.E. Martin, Thermodyn. 2 (IAEA, Vienna) (1966) 423.
[8] P. Blum, P. Guinet, H. Vaugoyau, CR Hebdom. Seances Acad. Sci. 257 (1963) 3401.
[9] P. Guinet, H. Vaugoyeau, P. Blum, French Atomic Energy Commission, Report CEA R3060, 1966.
[10] A. Pattoret, PhD thesis, Universite Libre de Bruxelles, 1969.
[11] S.P. Garg, R.J. Ackermann, J. Nucl. Mater. 88 (1980) 309.
[12] H.E. Cleaves, M.M. Cron, J.T. Sterling, Report CT2-618, 1945.
[13] C. Guéneau, V. Dauvois, P. Perodeaud, C. Gonella, O. Dugne, J. Nucl. Mater. 254 (1998) 158.
[14] M.J. Bannister, J. Nucl. Mater. 24 (1967) 340.
[15] J.L. Bates, Thermodyn. 2 (IAEA, Vienna) (1966) 73.
[16] R.E. Latta, R.E. Fryxell, J. Nucl. Mater. 35 (1970) 195.
[17] R.A. Hein, L.H. Sjodahl, R. Szwarc, J. Nucl. Mater. 25 (1968) 99.
[18] G. Kjaerheim, E. Rolstad, Institute for Energy Technology, Halden, Norway, Report HPR-107, 1969.
[19] T. Tachibana, T. Ohmori, S. Yamanouchi, T. Itaki, J. Nucl. Sci. Technol. 22 (1985) 155.
[20] A.E. Martin, R.K. Edwards, J. Phys. Chem. 69 (1965) 1788.
[21] R.J. Ackermann, E.G. Rauh, M.S. Chandrasekharaiah, J. Phys. Chem. 73 (1969) 762.
[22] A. Kotlar, P. Gerdanian, M. Dode, J. Chem. Phys. 64 (5) (1967) 862.
[23] A. Kotlar, P. Gerdanian, M. Dode, J. Chem. Phys. 64 (7–8) (1967) 1135.
[24] A. Kotlar, P. Gerdanian, M. Dode, J. Chem. Phys. 65 (4) (1968) 687.

[25] K. Hagemark, M. Broli, J. Inorg. Nucl. Chem. 28 (1966) 2837.
[26] P.E. Blackburn, J. Phys. Chem. 62 (1958) 897.
[27] L.E.J. Roberts, A.J. Walter, J. Inorg. Nucl. Chem. 22 (1961) 213.
[28] C. Picard, P. Gerdanian, J. Nucl. Mater. 99 (1981) 184.
[29] K. Kiukkola, Acta Chem. Scand. 16 (1962) 327.
[30] T.L. Markin, R.J. Bones, Report AERE-R4042 HL 62/2187 (C3), UK, 1962.
[31] Y. Saito, J. Nucl. Mater. 51 (1974) 112.
[32] D.L. Marchidan, S. Matei, Rev. Roum. Chimie 20 (11–12) (1975) 1365.
[33] F. Gronvold, J. Inorg. Nucl. Chem. 1 (1955) 357.
[34] B.E. Schaner, J. Nucl. Mater. 2 (1960) 110.
[35] S. Aronson, J. Belle, J. Chem. Phys. 35 (4) (1961) 1382.
[36] A.M. Anthony, R. Kiyoura, T. Sata, J. Nucl. Mater. 10 (1) (1962) 8.
[37] A.C. MacLeod, J. Chem. Thermodyn. 4 (1972) 699.
[38] M. Dode, B. Touzelin, Rev. Chim. Min. 9 (1972) 139.
[39] B. Belbeoch, J.C. Boivineau, P. Perio, J. Phys. Chem. Solids 28 (1967) 1267.
[40] W. Van Lierde, J. Pelsmaekers, A. Lecocq-Robert, J. Nucl. Mater. 37 (1970) 276.
[41] H. Inaba, K. Naito, J. Nucl. Mater. 49 (1973) 181.
[42] K. Naito, T. Tsuji, T. Matsui, J. Nucl. Mater. 48 (1973) 58.
[43] T. Sata, Bull. Tokyo Inst. Tech. 56 (36) (1963) 21.
[44] C. Picard, P. Gerdanian, J. Nucl. Mater. 126 (1984) 255.
[45] T. Ishii, K. Naito, K. Oshima, J. Nucl. Mater. 36 (1970) 288.
[46] H.R. Hoekstra, S. Siegel, L.H. Fuchs, et al., J. Phys. Chem. 59 (1955) 136.
[47] R.J. Ackermann, A.T. Chang, J. Chem. Thermodyn. 5 (1973) 873.
[48] T. Matsui, T. Tsuji, K. Naito, J. Nucl. Sci. Technol. 11 (5) (1974) 216.
[49] R.A. Hein, P.N. Flagella, J.B. Conway, J. Am. Soc. 51 (1968) 291.
[50] L. Leibowitz, L.W. Mishler, M.G. Chasanov, J. Nucl. Mater. 29 (1969) 356.
[51] M.H. Rand, R.J. Ackermann, F. Gronvold, F.L. Oetting, A. Pattoret, Rev. Int. Haut. Temp. Refract. Fr. 15 (1978) 355.
[52] J.K. Fink, J. Nucl. Mater. 279 (2000) 1.
[53] R.A. Hein, P.N. Flagella, Report GEMP-578, 1968.
[54] L. Leibowitz, M.G. Chasanov, L.W. Mishler, D.F. Fischer, J. Nucl. Mater. 39 (1971) 115.
[55] M. Bober, J. Singer, Nucl. Sci. Eng. 97 (1987) 344.
[56] P. Gerdanian, M. Dode, Extrait J. Chim. Phys. 171 (1965).
[57] A. Nakumura, T. Fujino, J. Nucl. Mater. 149 (1987) 80.
[58] M. Tetenbaum, P.D. Hunt, J. Chem. Phys. 49 (1968) 4739.
[59] N.A. Javed, J. Nucl. Mater. 43 (1972) 219.
[60] A. Dinsdale, SGTE Data for Pure Elements, Calphad 15 (1991) 317.
[61] B. Sundman, B. Jansson, J.O. Andersson, Calphad 9 (1985) 153.
[62] I. Ansara, B. Sundman, Scientific Group Thermodata Europe, in: P.S. Glaser, (Ed.), Computer Handling and Determination of Data, North Holland, Amsterdam, 1986, p. 154.
[63] B. Jansson, Report TRITA-MAC-0234, Royal Institute Technology, S10044 Stockholm 70, Sweden, April 1984.
[64] D.A. MacInnes, C.R.A. Catlow, J. Nucl. Mater. 89 (1980) 354.
[65] B.T.M. Willis, Nature 197 (1963) 755.
[66] M. Hillert, B. Jansson, B. Sundman, J. Ågren, Metall. Trans. A 16 (1985) 661.
[67] I. Grenthe, J. Fuger, R.J.M. Konings, R.J. Lemire, A.B. Muller, C. Nguyen-Trung, H. Wanner, Chemical Thermodynamics 1 – Chemical Thermodynamics of Uranium, Edited by H. Wanner and I. Forest, OECD, North Holland, Amsterdam, 1992, p. 30.
[68] G. Benezech, J.P. Coutures, M. Foex, Thermodyn. Nucl. Mater. Proc. 4th Symp., Vienna 1974, 1975, p. 337.
[69] W. Breitung, K.O. Reil, U.S. Nucl. Reg. Comm., Report NUREG-CR-4295, 1985, p. 1.
[70] D.J.M. Bevan, I.E. Grey, B.T.M. Willis, J. Solid. State Chem. 61 (1986) 1.
[71] R.J. Ackermann, E.G. Rauh, M.S. Chandrasekharaiah, Argonne National Lab., Report ANL-7048, 1965, p. 1.
[72] D.I. Marchidan, S. Matei, Rev. Roum. Chimie 17 (1972) 1487.
[73] D.I. Marchidan, S. Matei-Tanasescu, Rev. Roum. Chimie 18 (1973) 1681.
[74] D.I. Marchidan, S. Matei-Tanasescu, Rev. Roum. Chimie 19 (1974) 1435.
[75] G.E. Moore, K.K. Kelley, J. Am. Chem. Soc. 69 (1947) 2105.
[76] J.B. Conway, R.A. Hein, J. Nucl. Mater. 15 (1965) 149.
[77] A.E. Ogard, J.A. Leary, Thermodyn. Nucl. Mater., Vienna 651 (1967).
[78] D.R. Fredrickson, M.G. Chasanov, J. Chem. Thermodyn. 2 (1970) 623.
[79] K.C. Mills, F.H. Ponsford, M.J. Richardson, N. Zaghini, P. Fassina, Thermochim. Acta 139 (1989) 107.
[80] Y. Takahashi, M. Asou, J. Nucl. Mater. 201 (1993) 108.
[81] R.K. Edwards, M.S. Chandrasekharaiah, P.M. Danielson, High Temp. Sci. 1 (1969) 98.
[82] K. Gotoo, K. Naito, J. Phys. Chem. Sol. 26 (1965) 1679.
[83] E.F. Westrum, Y. Takahashi, F. Gronvold, J. Phys. Chem. 69 (1965) 3192.
[84] F. Gronvold, N.J. Kveseth, A. Sveen, J. Tichy, J. Chem. Thermodyn. 2 (1970) 665.
[85] H. Blanck, C. Ronchi, Acta Crystallogr. A 24 (1968) 657.
[86] P.O. Perron, report AECL-3072 (1968).
[87] C. Affortit, High Temp. High Press. 1 (1969) 27.
[88] C. Ronchi, G.J. Hyland, J. Alloys Comp. 213&214 (1994) 159.